Geophysical Journal International

Geophys. J. Int. (2014) **199,** 658–672 doi: 10.1093/gji/ggu293

GJI Geomagnetism, rock magnetism and palaeomagnetism

Haematite pigmentation events and palaeomagnetic recording: implications from the Pilbara Print Stone, Western Australia

Alexandra Abrajevitch,[1,2] Brad J. Pillans[1] and Andrew P. Roberts[1]

[1]*Research School of Earth Sciences, The Australian National University, Canberra, ACT* 0200*, Australia. E-mail: alexandra.abrajevitch@gmail.com*

[2]*Institute of Tectonics and Geophysics, Russian Academy of Sciences, Khabarovsk, Russia*

Accepted 2014 July 22. Received 2014 July 10; in original form 2014 February 10

SUMMARY

Haematite pigment is a common constituent of sedimentary rocks, but its contribution to the natural remanent magnetization of rocks is poorly understood. Here, we describe magnetic properties of two distinct pigment types that produce a characteristic decorative 'print stone' found in the ∼2.5 Ga Mount McRae Shale Formation, Hamersley Province, Western Australia. Distinct magnetic remanence directions observed in the Print Stone can be correlated to each pigment type. By comparison with the Australian apparent polar wander path, the remanence carried by uniformly distributed pigment can be dated to ∼15–25 Ma, while two age options, the Mesoproterozoic (∼1.5 Ga) or the middle Carboniferous (∼320–310 Ma), are permissible for the remanence carried by the pigment responsible for the distinctive 'newsprint' pattern. Magnetic properties and demagnetization characteristics of the different pigment types overlap significantly, and thus are not predictive of the dominant remanence carrier. Magnetic characteristics of the uniformly distributed pigment vary significantly on short spatial scales. Strong local control on pigment formation raises the possibility that a primary remanent magnetization may survive locally in pockets within sedimentary red bed formations.

Key words: Palaeomagnetism applied to geological processes; Remagnetization; Rock and mineral magnetism; Australia.

1 INTRODUCTION

Haematite is a common iron-oxide mineral that occurs as an accessory phase in a wide range of sedimentary and granitic rocks. It occurs in a variety of forms, as metallic masses (specularite), primary grains of magmatic origin or as fine-grained pigment. Haematite can carry a highly stable remanent magnetization that is resistant to partial heating as well as to chemical alteration under oxidizing conditions at Earth's surface (Dunlop & Özdemir 1997). In volcanic and metamorphic rocks, primary haematite grains can acquire a thermoremanent magnetization (TRM) on cooling through the Néel temperature (680 °C). Detrital haematite grains, when released by weathering processes, and then transported and deposited within sediments, can align their magnetic moments with the ambient geomagnetic field during deposition or shortly after, thus contributing to a depositional remanent magnetization (DRM). Acquisition of a TRM or a DRM is of interest in palaeomagnetism because the magnetization dates to the time of rock formation.

Haematite can also form through authigenic processes; by dehydration of goethite, as a result of pseudo-morphic replacement of magnetite (martitization), or by *in situ* chemical precipitation (e.g. Cornell & Schwertmann 2003). Authigenic haematite formation is often closely associated with water availability (e.g. Wagner *et al.* 2013), therefore, a chemical remanent magnetization (CRM) carried by authigenic haematite grains can sometimes be correlated to fluid migration events, such as exposure to meteoric precipitation (e.g. Ricordel *et al.* 2007), or to orogenic fluid flow episodes (e.g. Park 1997). In common palaeomagnetic practice, however, secondary haematite is usually considered an undesirable contaminant that obscures the primary TRM or DRM record.

The magnetic properties of pigmentary haematite and specularite, as a means of estimating the relative importance of CRM and DRM in red beds, have been investigated extensively (see Dunlop & Özdemir 1997 and Van der Voo & Torsvik 2012 for reviews). The partitioning of magnetic phases into pigmentary and detrital fractions in such studies usually involves either chemical leaching or mechanical disaggregation of sediments. Neither of these techniques can provide strict separation of remanence carriers, therefore, such studies tend to capture the main features, but not the full variability of magnetic properties of these two types of haematite. In this study, we have investigated the magnetic properties of natural haematite pigments formed by hydrothermal precipitation in host rocks that lack detrital magnetic phases. Accordingly, the observed magnetic properties can be directly attributed to authigenic pigments, which can help to understand the implications of pigmentation for recording palaeomagnetic signals.

2 SAMPLING

For this study, we sampled a distinct decorative stone known as Print Stone, or Newsprint Jasper, at the only known outcrop located in the Hamersley Basin, Western Australia (Fig. 1a). The Print Stone is a hard silicified shale (normally with pale buff colour) tinted by haematite pigment of two types; a purplish pigment that forms the distinct 'Newsprint' pattern and an orange-red pigment that locally creates a background to the Newsprint pattern (Figs 1b and c). The orange-red pigment occurs in wide patches that vary in hue and intensity throughout the outcrop; however, compared to the Newsprint type the distribution of this pigment is visually uniform on a decimetre scale and, for simplicity, we refer to this type of pigment as 'uniform'. Thirty-nine hand samples were oriented with a magnetic compass and an inclinometer. Our Pilbara print stone (PPS) collection includes the available range of newsprint and uniform pigment combinations. The bedding at this locality is subhorizontal.

For comparison, we collected fourteen shale samples with dark red haematite staining (Fig. 1d) from a road cut outcrop at Mount Nameless (Fig. 1a). To sample soft shales (TOM collection), small cube-shaped pedestals were carved from the outcrop face with a sharp knife and plastic boxes (8 cm^3 volume) were carefully fitted onto the pedestals. Before extracting the sample, the orientation of each box's surface was measured with a compass and inclinometer.

The sampled rocks belong to the Mount McRae Shale member of the early Palaeoproterozoic Hamersley Group that comprises banded iron formation (BIF) and shale formations. The 50-m-thick Mount McRae Shale is composed of carbonate and siliciclastic turbidites with thin beds of tuff and volcanic breccia; it locally contains large organic carbon and pyrite concentrations (Trendall & Blockley 1970; Harmsworth *et al.* 1990; Pickard *et al.* 2004; Raiswell *et al.* 2011). Re-Os bulk shale geochronology (Anbar *et al.* 2007) and ^{207}Pb–^{206}Pb zircon dating of a tuff layer (Rasmussen *et al.* 2005) constrain the depositional age to ~2500 Ma.

The uppermost 12 m of the formation is transitional to the Brockman Iron Formation, which consists of alternating sequences of BIF, shale and chert (Trendall & Blockley 1970; Harmsworth *et al.* 1990). The Brockman Iron Formation hosts economically important high-grade haematite ore deposits. These deposits are found in locations where iron-rich BIF host rocks are intersected by major faults with an extended history of hydrothermal fluid circulation (Taylor *et al.* 2001; Rasmussen *et al.* 2007). U-Pb dating of phosphate minerals that coprecipitated with haematite during mineralization indicates that these minerals grew during multiple discrete events, spanning more than 1 billion years (Rasmussen *et al.* 2007). The long-lived multistage mineralization process attests to the long history of iron-rich fluid migration in the region.

3 METHODS

In the laboratory, hand samples were cut into standard cubes with ~20 mm sides, which yielded 1–6 specimens per sample, and 126

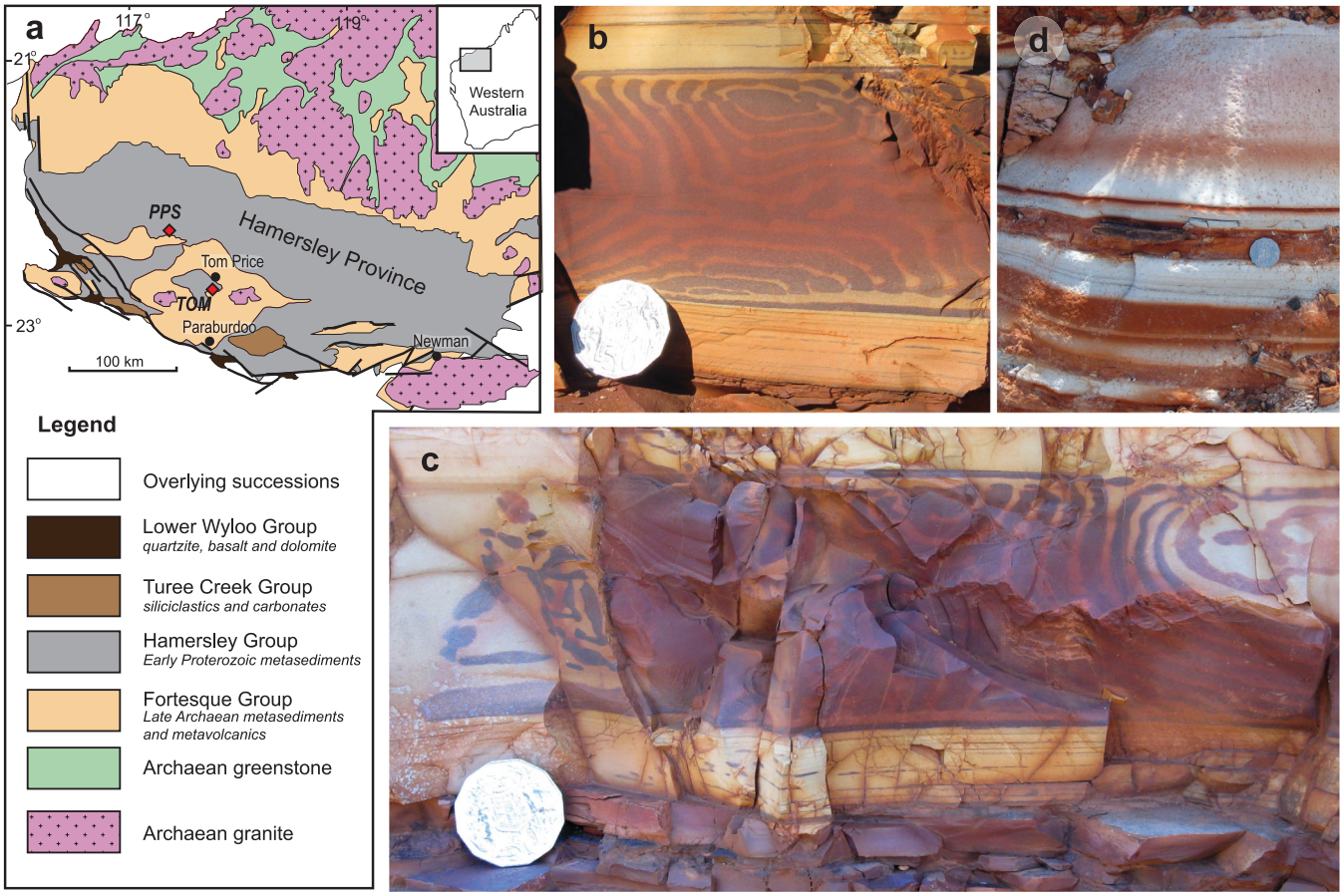

Figure 1. (a) Geological map of the Pilbara Craton modified from Rasmussen *et al.* (2007). Sampling localities are marked by rhombi; black circles mark locations of major iron ore deposits. (b–d) Pigment distribution examples for Print Stone (b and c) and TOM (d) localities. An Australian 50-cent coin (31.5-mm diameter) is shown for scale.

Table 1. Directions of characteristic remanent magnetization (ChRM) components for PPS samples.

Sample	ChRM type	*N*	Dec.	Inc.	*k*	α_{95}
pps-01	1	3	177.0	56.8	2436	
pps-02	1	2	188.3	52.4	153	
pps-03	2	3	210.6	61.6	89	
pps-04	1	3	185.6	56.3	908	
pps-05	2	2	214.0	78.0	1188	
pps-06	2	1	220.0	71.1		
pps-07	2	2	31.8	−69.8	2181	
pps-08	1	2	178.6	57.9	2587	
pps-11	2	3	50.5	−69.7	588	
pps-12	2	1	50.9	−72.4		
pps-12	1	3	11.9	−53.7	164	
pps-13	1	5	341.7	−58.5	618	
pps-14	1	4	345.6	−59.6	73	
pps-15	2	2	203.6	74.0		
pps-16	2	3	36.9	−61.7	512	
pps-17	1	4	7.4	−59.4	483	
pps-18	1	3	2.7	−37.0	166	
pps-19	1	2	354.2	−48.0	237	
pps-20	2	1	28.6	−67.8		
pps-20	1	4	3.9	−39.4	112	
pps-21	1	3	6.9	−53.5	437	
pps-22	2	3	61.6	−67.5	55	
pps-23	1	3	2.0	−42.9	1609	
pps-24	1	4	358.4	−55.9	154	
pps-25	1	3	358.1	−52.4	283	
pps-26	2	4	198.4	76.6	5435	
pps-27	2	4	184.6	70.8	285	
pps-27	1	2	359.8	−52.8	154	
pps-28	1	2	353.3	−52.5	104	
pps-29	2	3	234.9	67.6	472	
pps-30	2	3	208.3	70.9	431	
pps-31	1	3	349.1	−46.7	192	
pps-31	2	1	193.4	65.1		
pps-32	1	2	357.1	−50.2	659	
pps-33	1	6	0.8	−43.4	198	
pps-34	1	3	354.5	−29.7	256	
pps-35	1	3	177.0	35.5	1215	
pps-36	1	4	354.2	−30.9	369	
pps-37	1	4	352.2	−41.4	308.3	
pps-38	1	4	0.2	−42.7	372	
pps-39	2	2	33.7	−74.6	8675	
pps-40	1	5	174.0	51.8	504	
pps-41	1	2	182.7	59.6	3665	
Mean ChRM1		27	178.4	49.1	68	3.4
Mean ChRM2		16	214.3	70.6	133	3.2

Notes: N is the number of specimens; Dec. and Inc. are the declination and inclination of the site-mean direction (in °); $\alpha 95$ is the radius of the 95 per cent confidence cone about the mean direction (in °); *k* is the Fisher (1953) concentration parameter. Directions are given in geographic coordinates; no correction for tilt was applied because of subhorizontal bedding at the site.

specimens in total (Table 1). All magnetic measurements were made at the Australian National University palaeomagnetism laboratory. The natural remanent magnetization (NRM) of the specimens was measured with a 2-G Enterprises superconducting rock magnetometer equipped with in-line alternating field (AF) demagnetization coils. The specimens were progressively demagnetized using one of the following protocols. Sixty-seven specimens—approximately half of the collection—were thermally demagnetized (TH) in air in an ASC TD-48 oven. Temperatures were progressively increased in steps ranging initially from 50 °C at lower temperatures to 5 °C at higher temperatures until less than 5 per cent of the initial NRM intensity remained, up to a maximum temperature of 690 °C. The remaining samples were demagnetized using a combination of AF and thermal techniques. AF demagnetization proceeded at steps of 5– 20 mT up to a maximum peak field of 170 mT. Twenty-five specimens were first subjected to AF demagnetization, which was then followed by the standard TH procedure described above. The remaining 34 samples were heated to 200 °C prior to AF treatment; after completion of the AF sequence, TH continued until the NRM was completely demagnetized.

Throughout the demagnetization experiments, samples and instruments were housed in a magnetically shielded room with residual fields <300 nT. Demagnetization data are plotted on orthogonal demagnetization diagrams (Zijderveld 1967) and stereographic projections. Remanence directions were determined by principal component analysis (Kirschvink 1980) using the palaeomagnetic software package Remasoft 3.0 (Chadima & Hrouda 2006).

Magnetic characteristics of three representative samples of different pigment types—a 'Newsprint' pigment, a newsprint pattern on a red background (a combination of newsprint and uniform pigment types) and a uniform pigment—were evaluated with a set of rock magnetic measurements made with a Quantum Designs Magnetic Property Measurement System (MPMS). Values of saturation magnetization (M_s), saturation remanence (M_{rs}) and coercivity (B_c) were determined from hysteresis loops, measured from +7 to –7 T at 50.5 mT steps, after subtracting the paramagnetic contribution. The coercivity of remanence (B_{cr}) was obtained by demagnetizing M_{rs} in a stepwise increasing back field. Coercivity spectra of pigment samples were further evaluated with isothermal remanent magnetization (IRM) acquisition experiments. IRMs were imparted with 26 logarithmically scaled steps, up to a maximum peak field of 7 T. IRM acquisition curves were decomposed into coercivity components using the fitting program of Kruiver *et al.* (2001), which is limited to symmetric distributions in logspace.

Characteristic low-temperature magnetic behaviour of iron oxides, such as the magnetic phase (Morin) transition in haematite (Morin 1950) and enhanced remanence on cooling typical of goethite (Dekkers 1989; Liu *et al.* 2006), were used to assess the mineralogy and grain size distribution of pigment grains. For such measurements, an IRM was imparted at room temperature (300 K) in a 7 T field; the remanence was then measured in zero field during cooling from 300 to 10 K, followed by warming from 10 to 400 K and subsequently cooling back to 300 K.

First order reversal curve (FORC) diagrams (Pike *et al.* 1999; Roberts *et al.* 2000) were used to investigate magnetostatic interactions and domain states of pigment grains. FORC measurements were made with a maximum applied field of 800 mT using a Princeton Measurements Corporation vibrating sample magnetometer (VSM). Although this maximum field is insufficient to magnetically saturate haematite and goethite, and, thus, the measurements do not represent saturation properties, FORC diagrams are nevertheless useful for magnetic characterization using instruments with similar maximum applied fields (e.g. Roberts *et al.* 2006). To improve FORC signal-to-noise ratios, samples were measured multiple times (2–12 repetitions) and the FORC distributions were averaged. Each measurement run includes 300 FORCs measured with a field increment of 3.14 mT, an averaging time of 200 ms and a wait time of 1 s between successive measurements. FORC diagrams were processed using the software of Heslop & Roberts (2012) with a smoothing factor (SF) of 7.

4 RESULTS

4.1 Thermal demagnetization

During TH demagnetization, all samples had stable behaviour, with vector endpoints following a consistent trend. Lack of evidence for acquisition of spurious magnetizations, such as erratic trends at high temperature steps, suggests that no metastable phases contribute to the NRM.

4.2 AF demagnetization

The samples subjected to combined AF and thermal demagnetization have variable response to AF demagnetization. In samples dominated by the Newsprint type of pigment, less than 1 per cent of the initial NRM was removed by AF demagnetization at maximum applied fields of 170 mT (e.g. Fig. 2, pps11–3). In samples with a red background (i.e. a significant content of the uniform pigment), the remanence loss during AF demagnetization ranges from zero up to ∼50 per cent. Often, sister specimens from the same hand sample have a widely variable contribution from the low coercivity fraction, as illustrated for three specimens of sample pps01 in Fig. 3.

AF demagnetization of a fresh specimen (pps01–2) reveals a component with a direction of Dec. = 176.5°, Inc. = 54.3° (MAD = 1.8°) and intensity of 0.36 mA m^{-1} in the 80–170 mT range (Fig. 3). Heating the sample to 100 °C after AF treatment uncovers an antipodal remanence component with Dec. = 360.0°, Inc. = –56.6° and similar magnitude of 0.41 mA m^{-1}. The characteristic remanent magnetization component (ChRM) with Dec. = 176.7°, Inc. = 57.0° (MAD = 2.3°), Int. = 1.25 mA m^{-1} was then revealed in the 250–690 °C temperature range. Initial heating of specimen pps01–3 to 200 °C reveals a magnetization component

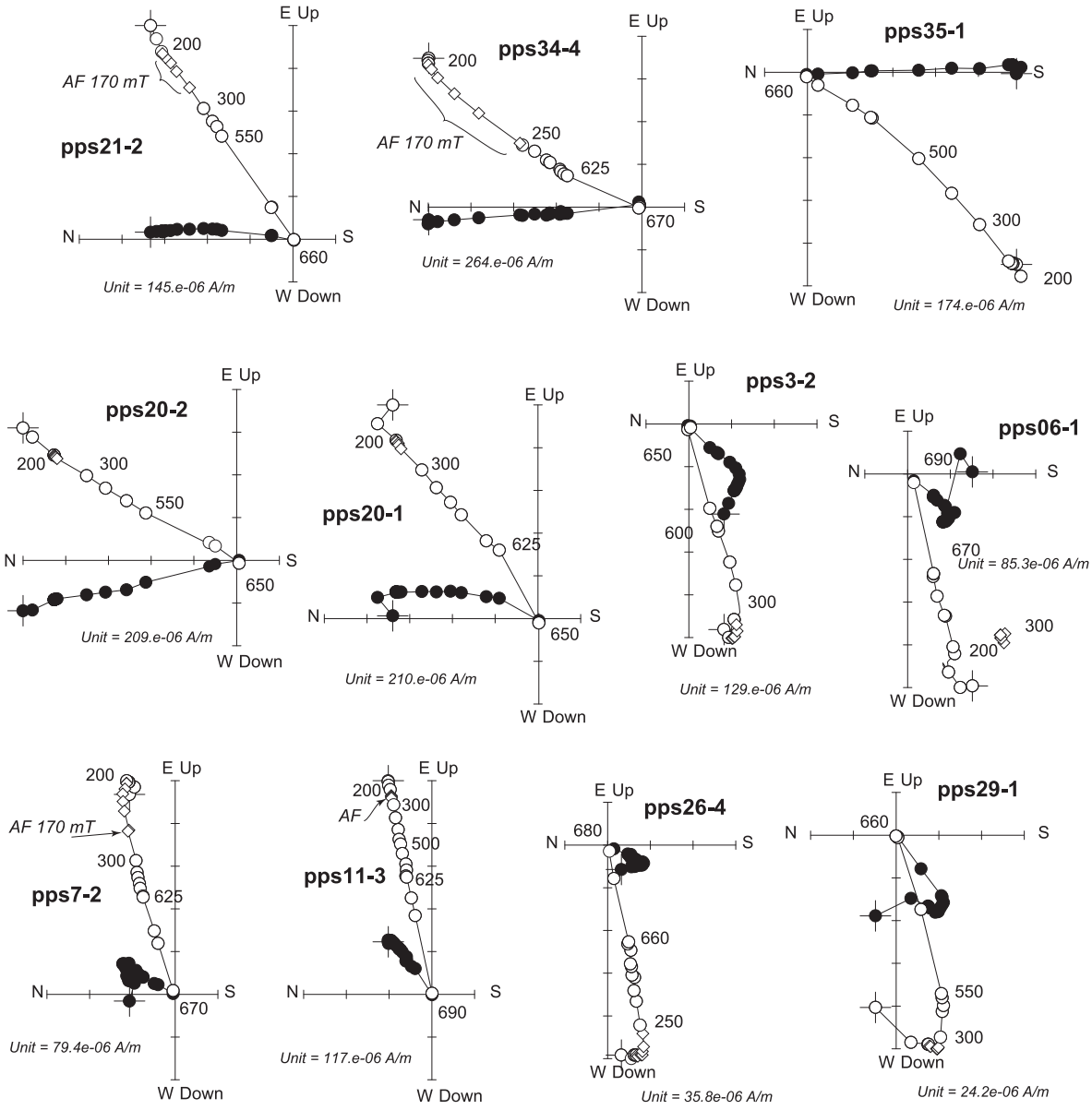

Figure 2. Representative examples of vector component diagrams for PPS samples, in geographic coordinates. Circles correspond to data from thermal demagnetization, while rhombi indicate data from AF demagnetization. Solid and open symbols represent endpoints projected onto the horizontal and vertical planes, respectively.

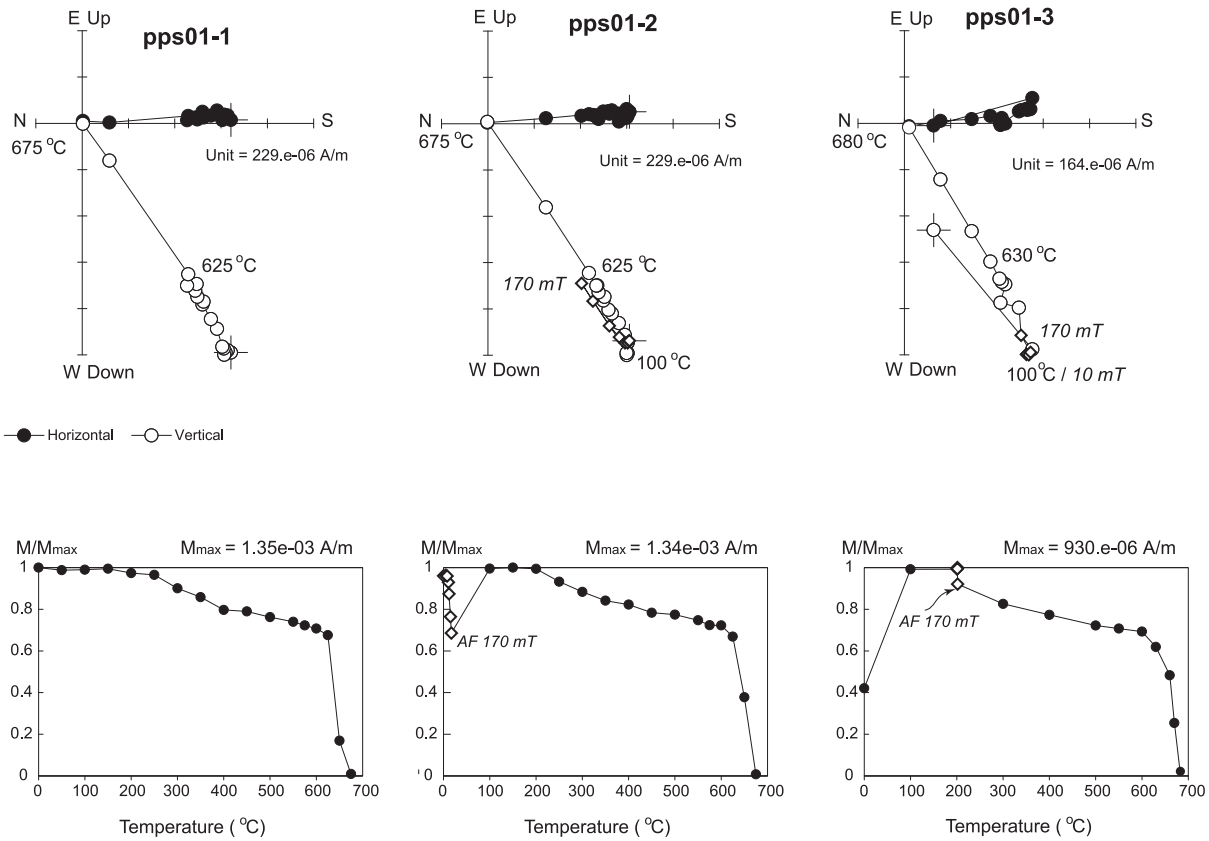

Figure 3. Vector component diagrams in geographic coordinates (upper row) and the corresponding normalized intensity curves (lower row) for three sister specimens from sample pps01. Circles correspond to thermal demagnetization data, while rhombi indicate AF demagnetization data. Solid and open symbols represent endpoints projected onto the horizontal and vertical planes, respectively.

with Dec. = 344.3°, Inc. = –49.4° and intensity of 0.53 mA m^{-1} (Fig. 3). Subsequent AF demagnetization to 170 mT removed only a small remanence component of 0.067 mA m^{-1}, leaving the ChRM with a direction of Dec. = 178.1°; Inc. = 58.4° (MAD = 2.3°) and intensity of 0.67 mA m^{-1}. For specimen pps01–1, which was subjected to TH demagnetization only, little (<1 per cent) of the NRM was lost on heating to 100 °C. The ChRM was unblocked in the 400–690 °C range and has a direction of Dec. = 177.2°; Inc = 55.9° (MAD = 2.2°); Int. = 1.02 mA m^{-1} (Fig. 3).

Overall, three magnetization components contribute to the NRM of sample pps01. A low coercivity (affected by AF demagnetization) remanence, a high-coercivity and low-unblocking-temperature component (i.e. not affected by AF demagnetization but removed at low temperature steps) and a high-coercivity high-unblocking-temperature component. Based on these characteristics, we identify the high-coercivity and low-unblocking-temperature component as goethite, and the high-coercivity high-unblocking-temperature component as haematite. The identity of the low coercivity magnetic carrier is less certain. Remanence carried by common low coercivity minerals such as magnetite and maghemite is known to be mainly removed by 100 mT (e.g. Dunlop & Özdemir 1997), while in our samples a larger fraction of the remanence is lost in the 120–170 mT range compared to the 0–100 mT range. We, therefore, conclude that the low coercivity remanence in the studied samples most likely resides in fine-grained haematite.

In the PPS sample collection, goethite invariably carries a magnetization with a direction close to that of the present-day field (PDF) at the sampling locality. The contribution of goethite to the NRM can be significant (e.g. up to 30 per cent of the NRM in specimen pps 01–2) but varies widely between samples (compared to the negligible contribution of goethite in specimen pps01–1). The direction of the low coercivity (fine haematite) component is usually close to that of the high-unblocking-temperature haematite component in the same sample. The ChRM seems to be equally well isolated by all demagnetization procedures.

4.3 Remanence components

Samples dominated by the Newsprint pigment usually have a single well-defined magnetization component (e.g. Fig. 2, pps11–3), while samples with the red background have two or three magnetization components. TH demagnetization only and heating to 200 °C followed by AF demagnetization tend to isolate two magnetization components (e.g. Fig. 3, pps01–3); the third component is only revealed by the initial AF followed by thermal treatment (e.g. Fig. 3, pps01–2). The presence of two magnetization components is evident in changing trends on vector end-point diagrams (Fig. 2). The component removed at lower temperature steps is designated as the low-temperature component (LTC). Unblocking temperatures for the LTC vary from 100 °C (e.g. Fig. 3) to ∼300 °C (e.g. Fig. 2, pps06–1). Its intensity, and thus its contribution to the total NRM, also varies. LTC directions are close to the PDF direction at the sampling locality (Fig. 4a).

The minimum unblocking temperature of the ChRM component ranges from ∼200 °C (e.g. Fig. 2, pps11–3) to 625 °C (e.g. Fig. 2, pps20–1). The ChRM directions fall into two populations, each

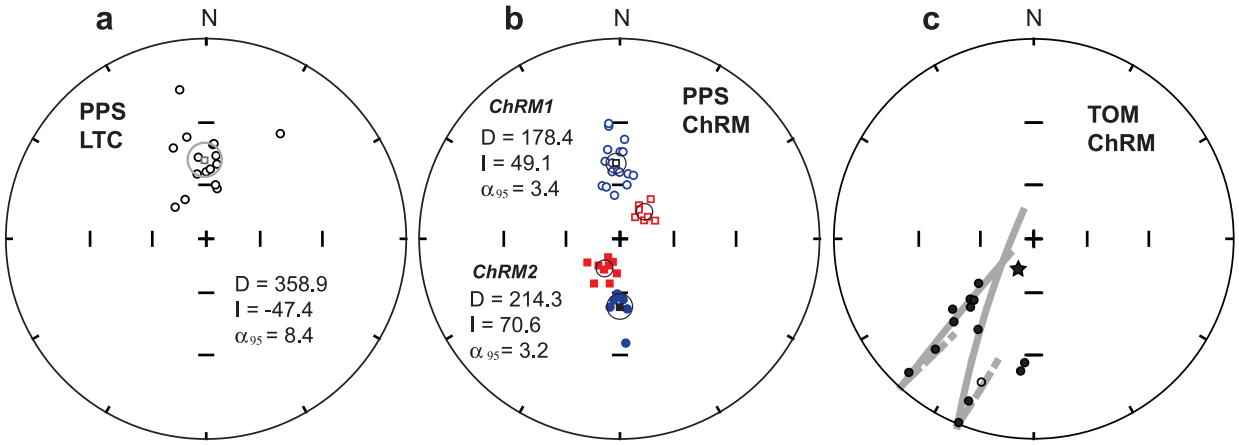

Figure 4. Sample-mean directions of the low-temperature component (LTC) (a) and characteristic remanent magnetization component (b) for the PPS samples. ChRM1 directions in (b) are shown with circles, while ChRM2 directions are represented by squares. (c) Directions of high-temperature (characteristic) components for individual samples of the TOM collection. Fitted great circle trajectories are shown with grey lines. The star corresponds to the mean ChRM2 direction for the PPS collection. Open and solid symbols are projections onto the upper and lower hemispheres, respectively. All directions are shown in geographic coordinates.

consisting of antipodal groups (Fig. 4b). The first group (ChRM1; circles in Fig. 4b) has northerly declinations with intermediate negative inclinations; the second group (ChRM2; squares in Fig. 4b) is characterized by northeasterly declinations, and generally steeper negative inclinations. Both populations pass the reversal test of McFadden & McElhinny (1990) with the observed angular distance between the mean directions of the two polarities (γ_o) being smaller than the critical (γ_c) value; $\gamma_o = 5.51 < \gamma_c = 7.68$ for ChRM1, and $\gamma_o = 5.07 < \gamma_c = 6.26$ for ChRM2. The ChRM type can vary between sister specimens from the same hand sample (e.g. Fig. 2, pps20–1 and pps20–2), and correlates with background colouration. ChRM2 is found in specimens dominated by the Newsprint pigmentation on a white or light pink background, while ChRM2 is common in specimens with the darker background colour.

In some specimens, in addition to a well-defined LTC and ChRM, a change in vector-endpoint trajectories is observed in the 250 to ∼400–600 °C temperature range (e.g. Fig. 2, pps35–1, pps20–1 and pps29–1). Such a change can be interpreted as due to the presence of an intermediate temperature component. In all such cases, however, the direction of the intermediate component lies on a great circle between the LTC and ChRM for the specimen, which is typical of a composite magnetization. Although such intermediate directions occasionally resemble that of ChRM1 (e.g. Fig. 2, pps20–1), this is likely to be a coincidence because the relationship is not universal (e.g. Fig. 2, pps29–1). We regard such intermediate directions as composite magnetizations and do not include them in our estimates of the mean ChRM direction.

4.4 TOM samples

The TOM samples have consistent demagnetization behaviour. A low-temperature component with random directions is removed by thermal demagnetization at 100–300 °C. Above 300 °C, a ChRM decays linearly to the origin of the demagnetization diagrams. ChRM directions are well defined (MAD < 5°), but have a large spread in declination and inclination values (Figs 4c and 5). ChRM directions from 12 samples define two great-circle trajectories that converge onto a direction that is close to the mean ChRM2 direction from the PPS collection (marked by a star in Fig. 4c).

4.5 Unblocking temperature spectra

The maximum unblocking temperature (Tb_{max}) of the ChRM, determined as the temperature at which the magnetization decreases to zero, ranges between ∼625 and 690 °C for the PPS samples and between ∼625 and 650 °C for the TOM samples (Fig. 6). The majority of the PPS specimens have 'blocky' magnetization vs. temperature curves that are typical of haematite, with little remanence removed between 300 and 500–550 °C and a major loss of remanence within 50 °C of the Néel temperature. There is no systematic difference in Tb_{max} between samples that carry ChRM1 (dashed line in Fig. 6a) and ChRM2 (solid line in Fig. 6a). In the TOM samples, the remanence loss on heating is more gradual, although some samples have a similar stepwise drop in magnetization intensity on approach to the Néel temperature (Fig. 6b).

5 ROCK MAGNETISM

5.1 Hysteresis parameters

The magnetization of shales with light-colour matrix has a linear dependence on applied field (Fig. 7), which is typical of paramagnetic materials. Differences in the slope of M(B) curves between matrix shale samples indicate differences in paramagnetic mineral composition and/or concentration. The lack of hysteresis attests to the absence of detrital ferrimagnetic matrix phases. Hysteresis loops of pigmented samples (shown in Fig. 8a in the ±1 T field range for clarity) are wide; no 'wasp-waisted' constriction in the middle is observed (that would suggest distinct populations with strongly contrasting coercivities; Roberts *et al.* 1995; Tauxe *et al.* 1996). Concentration-independent parameters M_r/M_s, coercivity B_c and coercivity of remanence B_{cr} are highest in the Newsprint pigment type, and are lowest in the uniform pigment (Tom07), while the 'Newsprint on a dark background' sample has intermediate values (Table 2). The remanent magnetization and coercivity of haematite grains depends on grain size (Stoner & Wohlfarth 1947), shape (e.g. Dang *et al.* 1998) and internal structure of (polycrystalline) particles (e.g. Rath *et al.* 1999). The higher coercivity of the Newsprint pigment compared to the uniform pigment could, for example, indicate a higher effective particle size, difference in morphology

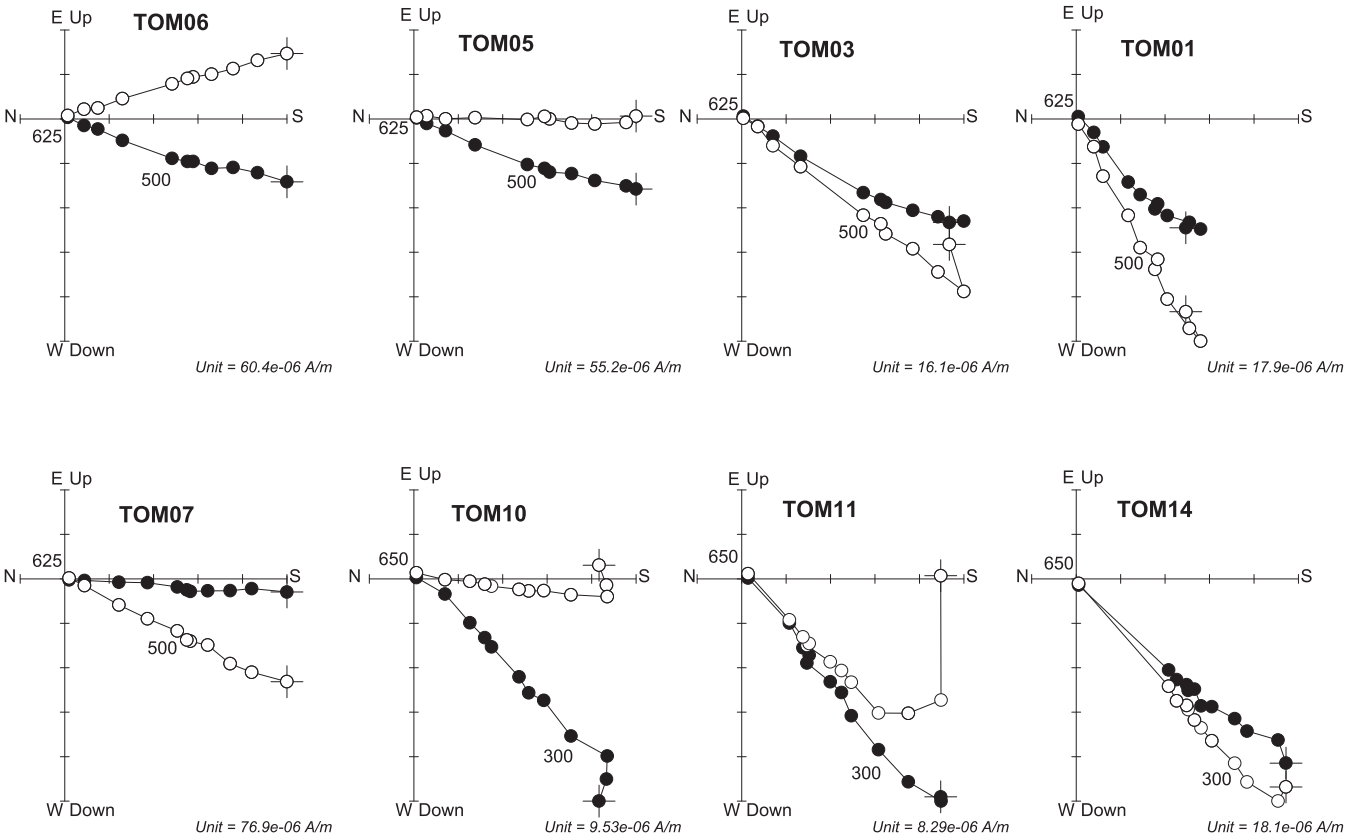

Figure 5. Representative examples of vector component diagrams for the studied TOM samples, in geographic coordinates. Solid and open symbols represent endpoints projected onto the horizontal and vertical planes, respectively.

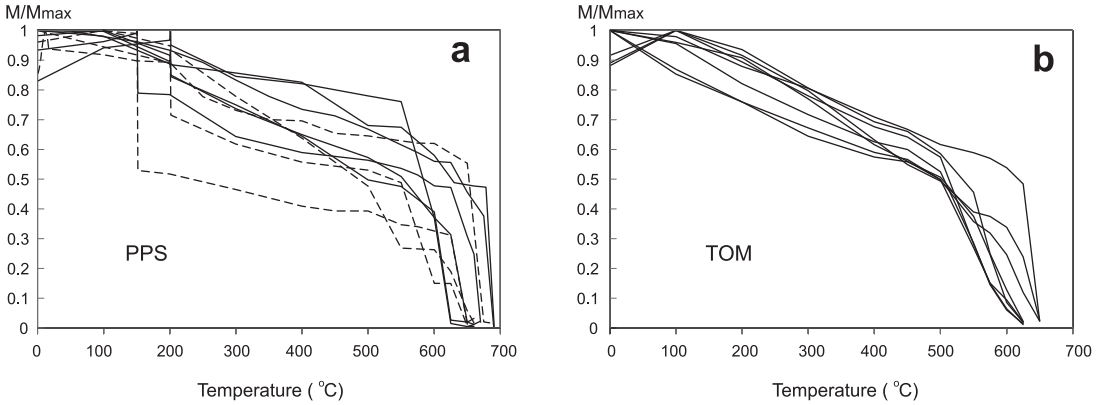

Figure 6. Normalized NRM intensity after stepwise thermal demagnetization for selected PPS samples (a) and for TOM samples (b). In (a), demagnetization curves for samples that carry the ChRM1 component are shown with dashed lines, while solid lines represent samples that carry the ChRM2 component.

(e.g. rhombohedral, pseudocubic, spherical or elongated grains), or different packing, with smaller distances between pigment grains leading to increased exchange interactions. Intermediate hysteresis parameter values for the 'Newsprint on a dark background' sample likely reflect a mixture of the two (Newsprint and uniform) pigment types.

5.2 IRM acquisition

Coercivity spectra of the three pigment types represented by gradient of IRM acquisition curves are shown in Fig. 8(b). Compared to the uniform pigment, the Newsprint pigment has a higher mean coercivity (represented by the field value at the peaks in Fig. 8b) and a narrower gradient IRM acquisition peak. The mean coercivity values that exceed 250 mT (logB = 2.4) are typical of haematite (e.g. Robertson & France 1994). The narrower shape of the Newsprint pigment peak (the restricted coercivity range) is indicative of more uniform grain sizes and/or compositions (e.g. Robertson & France 1994). The narrow coercivity spectra, with a smaller proportion of low coercivity particles in the Newsprint pigment particles (Fig. 8b, pps11), explains the inefficiency of AF demagnetization in Newsprint-dominated samples compared to a relatively large loss of remanence in samples with a dark background (i.e. the uniform pigment). The noticeable high coercivity

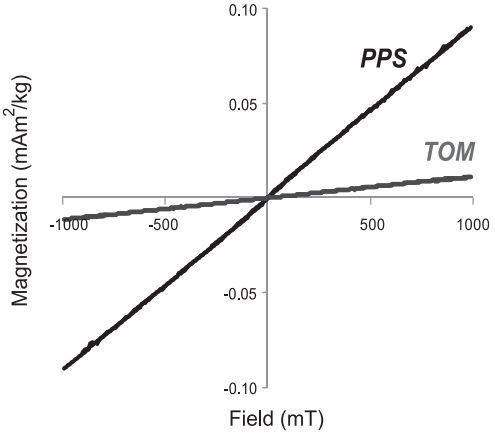

Figure 7. Field dependence of magnetization for representative matrix shale samples for the PPS and TOM samples.

tail (<1000 mT, log$B$ = 3) in the uniform pigment (Fig. 8b, TOM07) suggests a contribution from a high-coercivity phase, likely goethite. The coercivity spectrum of the 'Newsprint on a dark background' sample (Fig. 8b, pps25) is intermediate between the Newsprint and uniform pigment types.

5.3 Low-temperature cycling

Low-temperature behaviour of the studied samples varies significantly (Fig. 8c). None of the samples has a clear expression of the Morin (Morin 1950) transition for haematite that is usually manifested as a sharp loss of remanence on cooling at 250–260 K with a partial remanence recovery on warming (e.g. Özdemir *et al.* 2008). In the Newsprint pigment, the loss of remanence instead is gradual, spanning the ∼235 to 10 K temperature range, with little recovery in magnetization on warming back to room temperature. The Morin transition is known to be sensitive to crystallinity, extent of cation substitution and grain size of haematite particles. In chemically pure samples, the transition temperature shifts to lower temperatures with decreasing haematite grain-size until it completely disappears in grains smaller than 30 nm (Özdemir *et al.* 2008). Assuming that the haematite is nearly stoichiometric, the broad Morin transition observed for samples with the Newsprint pigment indicates the presence of haematite grains with a wide range of sizes, from ∼30 to ∼600 nm. The continuing loss of remanence on the high temperature limb (300 K = >400 K) with partial remanence recovery on cooling 400 K = >300 K is indicative of the presence of particles close to the superparamagnetic (SP) threshold size of ∼20 nm (Özdemir *et al.* 2008).

The low-temperature behaviour of the 'intermediate' dark background sample (pps–25) is generally similar to that of the Newsprint sample. However, a more gentle slope on cooling and a smaller remanence loss indicates a much stronger suppression of the Morin transition, likely due to the smaller fraction of pigment grains exceeding 30 nm in size. In contrast to the previous examples, the magnetization of samples with the uniform pigment increases on cooling to 10 K. The rise in magnetization is essentially reversible, with the remanence recovering its intensity on the return to 300 K. A distinct kink in the slope of the warming curve is observed at ∼360 K, and the remanence loss on heating from 300 to 400 K is not recovered on cooling back to 300 K. The reversible remanence increase on cooling accompanied by non-recoverable remanence loss on warming through ∼360 K (the Néel temperature) is a characteristic signature of goethite (e.g. Carter-Stiglitz *et al.* 2006; Liu *et al.* 2006). The observed Néel temperature, which is lower than typical of stoichiometric goethite ∼ 120 °C (Özdemir & Dunlop 1996), is indicative of structural or compositional defects in goethite grains (e.g. Liu *et al.* 2006). The contribution of goethite to the IRM of the uniform pigment (estimated as the remanence loss in the 300 K = >400 K = >300 K cycle after Carter-Stiglitz *et al.* (2006), although some fraction this remanence loss can be due to SP haematite) is 2.34 mAm^2 kg^{-1}, or ∼13 per cent of the total IRM.

Although slight separation between the cooling and warming curves in the 300 K = >10 K = >300 K low-temperature cycle may indicate a severely suppressed Morin transition, the bulk of the uniform pigment lacks a Morin transition. Assuming near-stoichiometry of uniform pigment haematite grains, this suggests a narrow grain-size range of ∼20 nm (around the SP threshold size) to ∼30 nm for the remanence carrying grains. This narrow estimated size range, which is smaller than that estimated for the Newsprint pigment, is, however, inconsistent with the wider coercivity spectra observed for the uniform pigment. Such a narrow particle size distribution should also give rise to wasp-waisted hysteresis (e.g. Tauxe *et al.* 1996), which we did not observe (Fig. 8a, pps25, TOM07). More likely, therefore, suppression of the Morin transition in the uniform pigment reflects a higher density of structural and compositional defects rather than grain size variations.

5.4 FORC distributions

A FORC diagram describes the distribution of coercivities and local interaction fields for an assemblage of magnetic particles (Pike *et al.* 1999; Roberts *et al.* 2000). Vertical spread in a FORC distribution is a manifestation of magnetostatic interactions, while the B_c coordinate at the peak of each distribution is a measure of the modal coercivity of the particle assemblage. FORC distributions for the studied pigment types have similar peak coercivity ranges with modal coercivity (B_c coordinate of the distribution peak) of 140–200 mT (Fig. 9b); these values are typical of (non-saturated) haematite (e.g. Roberts *et al.* 2006). The highly elongated non-zero FORC distributions for the Newsprint samples (Fig. 9a) are typical of single domain (SD) particle systems (e.g. Pike *et al.* 1999; Roberts *et al.* 2000). A vertical cross-section through the peak of the FORC distribution (Fig. 9c) is narrow, which is typical of highly dispersed particle systems, but somewhat skewed, which suggests the presence of two grain populations. A large narrow peak centred at the B_u = 0 axis suggests that a large fraction of the particles are well isolated and unaffected by interactions. A smaller wider peak is indicative of a population of small particle clusters within which there are strong but localized magnetostatic interactions (e.g. Pike *et al.* 1999).

In contrast, the FORC distribution peak for the uniform pigment is wide and displaced below the B_u = 0 axis (Figs 9a and c). The wider vertical spread of contours is indicative of substantial random local interactions (due to particle clusters), while downward displacement of the peak indicates a stabilizing mean interaction field that acts parallel to the net magnetization of the sample (e.g. Pike *et al.* 1999; Roberts *et al.* 2000). Such distributions are typical of strongly interacting, that is, tightly packed, particle systems.

The FORC distribution for the 'Newsprint on a dark background' has characteristics that are intermediate between the previous two pigment types. The vertical spread is wider than in the Newsprint sample, but narrower than in the uniform pigment (Figs 9a and c). Similar to the uniform pigment, the FORC distribution peak is

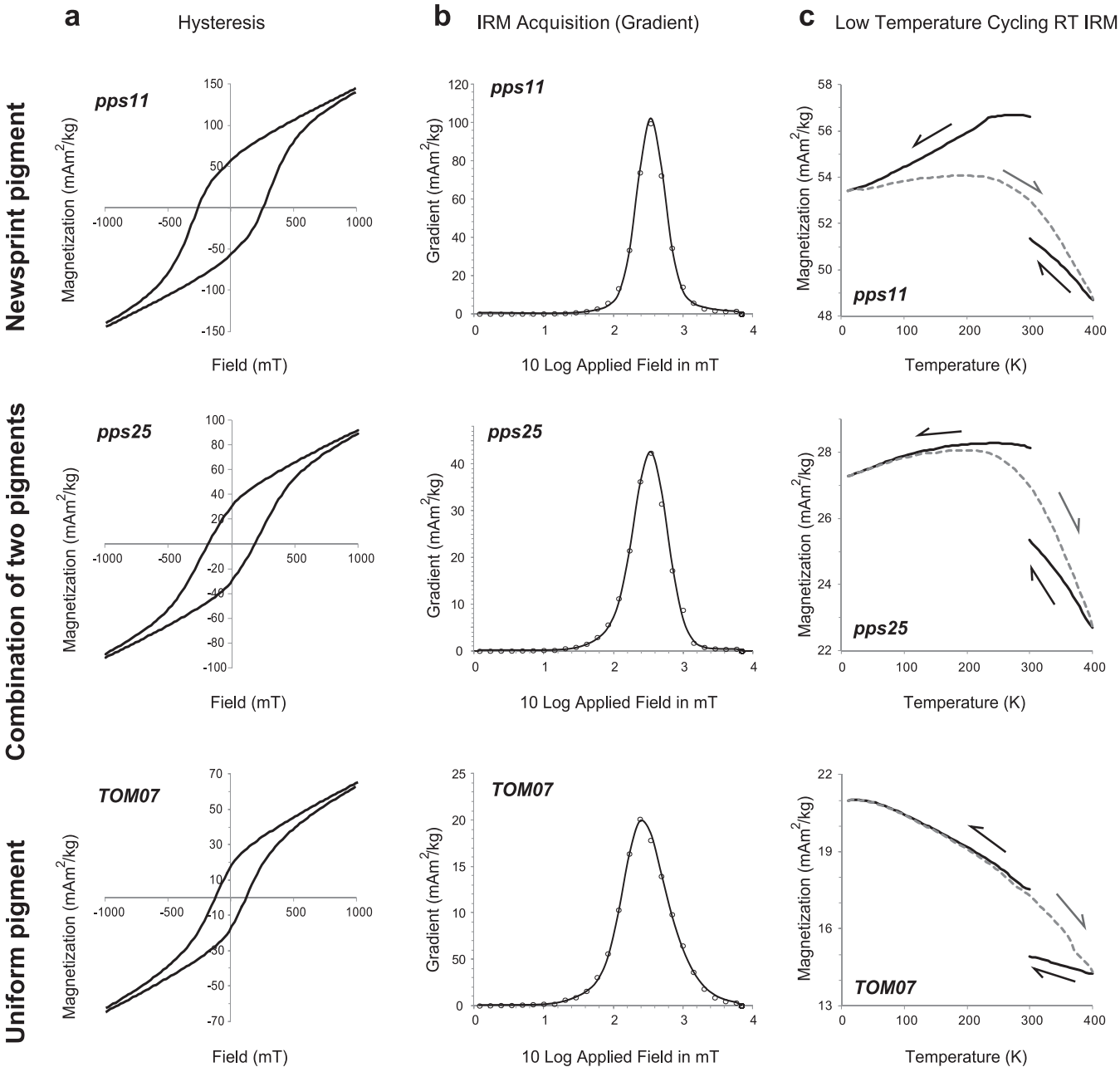

Figure 8. Rock magnetic characteristics: hysteresis loops (a), gradient IRM acquisition curves (b), and low-temperature dependence of magnetization (c) for three samples representative of the Newsprint pigment (pps11), a combination of the newsprint and uniform pigment (pps25), and uniform pigment (TOM07).

Table 2. Hysteresis parameters for the representative pigment types.

Pigment type	M_r (mAm^2/kg^{-1})	M_s (mAm^2/kg^{-1})	M_r/M_s	B_c (mT)	B_{cr} (mT)
Newsprint pigment (pps11)	57.0	84.0	0.68	259.6	348.5
Newsprint+uniform (pps25)	30.2	53.5	0.56	238.4	322.0
Uniform (TOM07)	17.5	37.7	0.46	154.7	266.4

displaced below the $B_u = 0$ axis, but the displacement is smaller, indicating a smaller mean interaction field (Figs 9a and c).

In combination, rock magnetic characteristics indicate compositional variations among different pigment types. The Newsprint pigment is dominated by isolated non-interacting haematite grains that range in size from ~20 to ~600 nm, with small populations of particle clusters, and a negligible goethite content. In contrast, the uniform pigment consists of closely spaced, strongly interacting particles, and contains an appreciable amount of goethite in addition to poorly crystalline haematite. A combination of these two distinct pigment types in the 'Newsprint pattern on a dark background' samples gives rise to 'intermediate' magnetic properties.

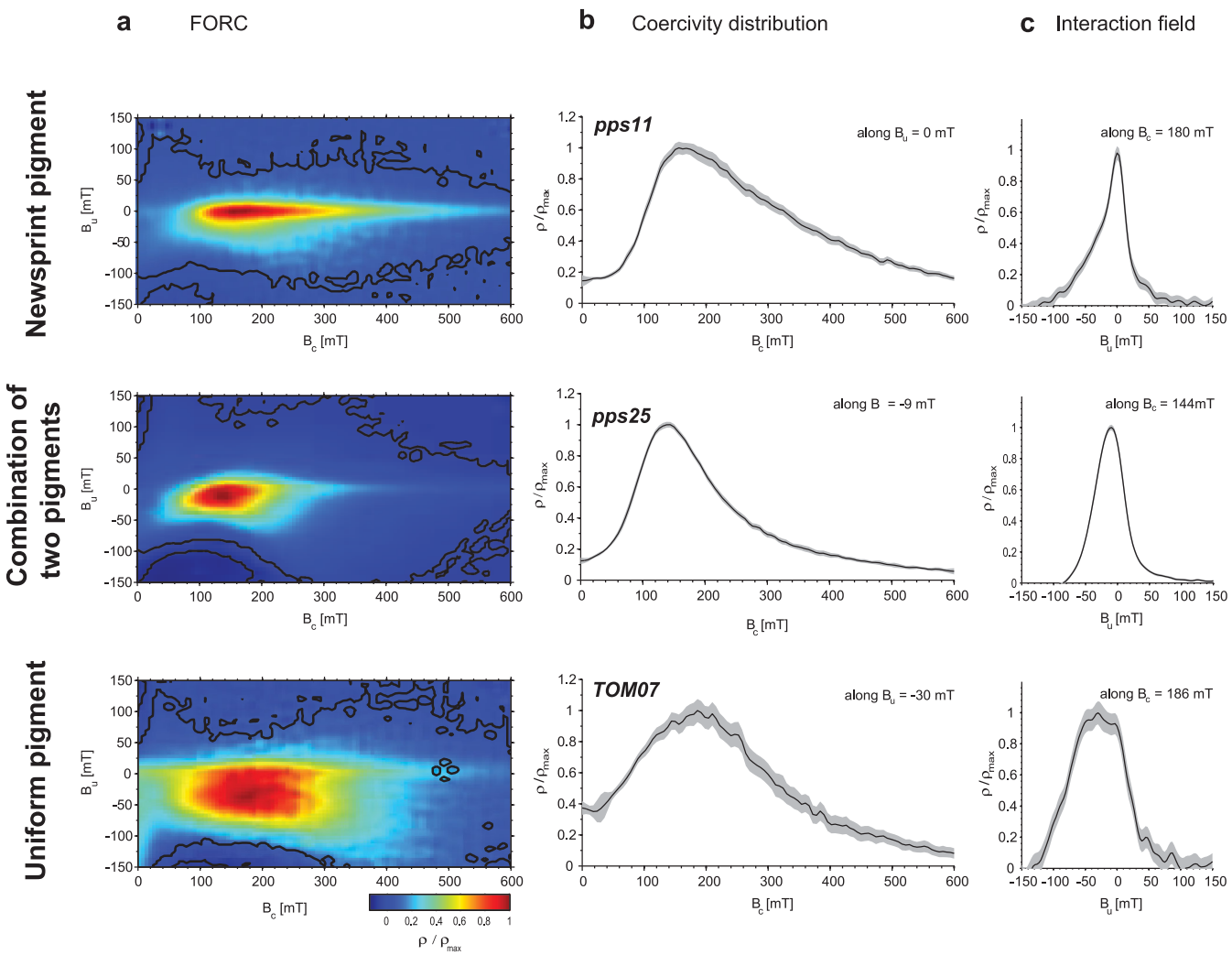

Figure 9. FORC diagrams (a) with profiles of the coercivity (b) and interaction field (c) distributions through the peak of the FORC distributions for representative pigment types (SF = 7 in all cases).

6 DISCUSSION

6.1 Magnetization age

The remanent magnetization of chemically precipitated haematite grains records the ambient geomagnetic field direction at the time of grain growth through a critical magnetic blocking volume (Kobayashi 1962). The age at which a particular pigment acquired its remanent magnetization can be roughly estimated by comparison with published records of palaeogeomagnetic field behaviour, that is by comparing the obtained palaeomagnetic pole with the trajectory of palaeomagnetic poles of known age (an apparent polar wander path, or APWP) for the continent or crustal block that contains the sampling localities.

The directions of the low-temperature components isolated from our PPS samples are close to the PDF direction at the sampling site, thus this magnetization is likely to be of recent origin. The mean ChRM1 direction is also close to the PDF direction, but it has a somewhat steeper mean inclination. The presence of reversed polarity directions that are antipodal to these normal polarity directions indicates that the ChRM1 remanence predates the ∼780 ka Matuyama-Brunhes geomagnetic reversal. Comparison with the well-defined global APWP in Australian coordinates (Torsvik *et al.* 2008) suggests a ∼15–25 Ma age for the ChRM1 direction (Fig. 10a). Precipitation of the uniform pigment is, thus, temporally coincident with formation of large channel iron ore deposits in the region (Macphail & Stone 2004; Danišík *et al.* 2013). This episode of iron mobilization is thought to have been linked to increased rainfall during Late Oligocene–Early Miocene global warming (e.g. Macphail & Stone 2004). Percolation of meteoric waters enriched in iron through the near-surface rocks at that time was likely responsible for the uniform pigment deposition.

Our ChRM2 palaeopole, however, deviates significantly from the APWP for the past 250 Ma (Fig. 10a), which suggests an older age for the Newsprint pigment. A number of Precambrian poles have been previously reported from the large iron ore deposits of the Hamersley province of the Pilbara craton (Table 3, Fig. 10b). A consistent group of remanence directions reported from the Mount Tom Price, Paraburdoo and Mount Newman ore bodies and host BIF (Table 3) has been attributed by Li *et al.* (1994) to a pervasive magnetic overprint that affected the Hamersley basin at ∼1.8 to 1.7 Ga. Apart from this prominent (presumably 1.8–1.7 Ga overprint) direction, Li *et al.* (2000) also reported a steep downward magnetic direction (named HP1) from high-grade haematite ores from the eastern Hamersley province (Table 3; Figs 10b–d). Based

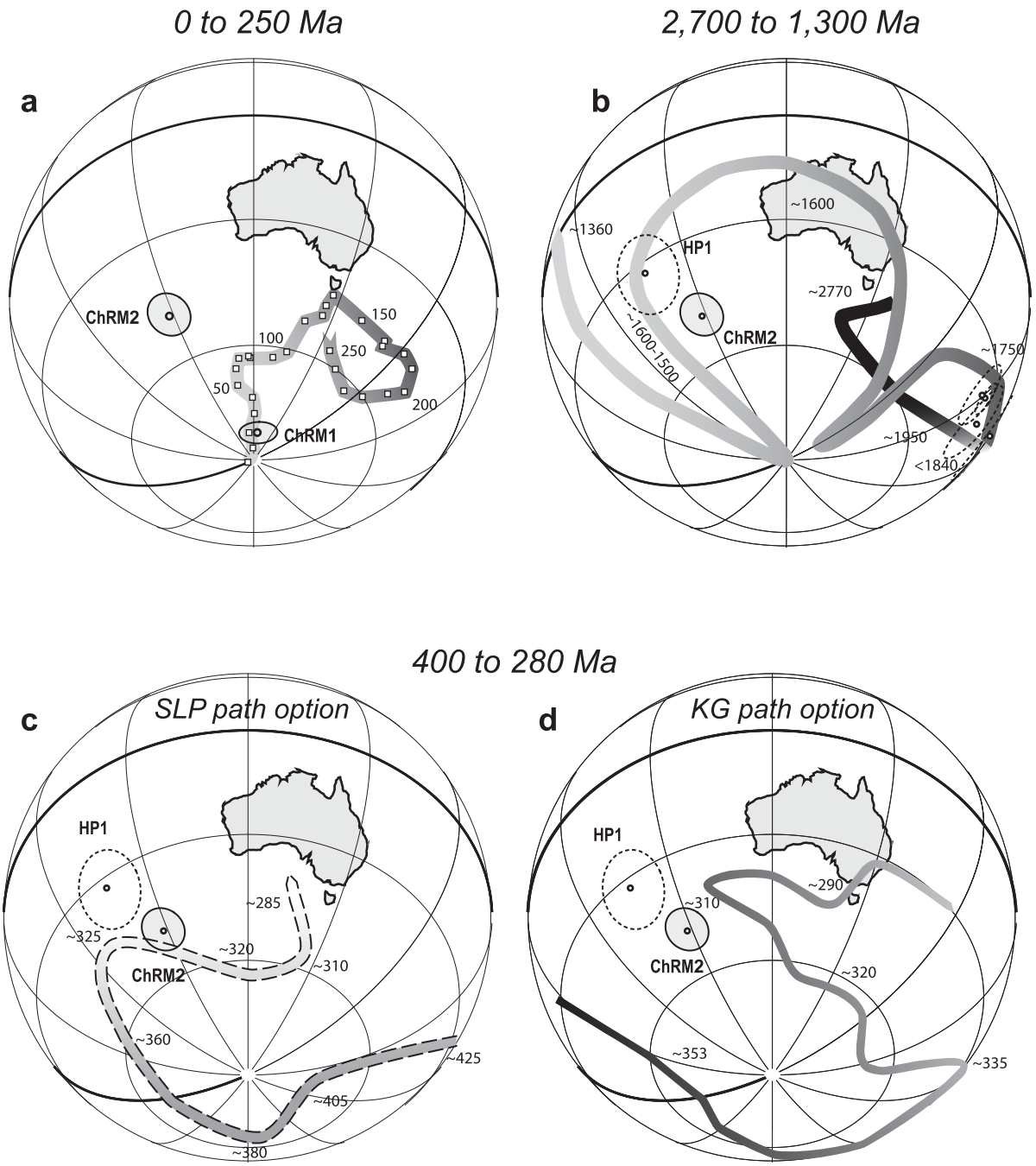

Figure 10. Comparison of palaeomagnetic poles for the ChRM1 and ChRM2 components from the Pilbara Print Stone with the reference APWP for Australia. (a) Post-250 Ma global APWP in Australian coordinates (Torsvik *et al.* 2008); (b) Proterozoic APWP of Wingate & Evans (2003) and two alternative early–middle Palaeozoic paths: (c) SLP-type (after Anderson *et al.* 2004), and (d) KG (Klootwijk 2010). Palaeomagnetic poles reported from iron ore deposits in the region (listed in Table 3) are shown for comparison with dashed confidence circles.

on a negative fold test, Li *et al.* (2000) inferred that the HP1 direction post-dates the ∼1.8–1.7 Ga Capricorn orogeny. A comparison with the APWP of the north Australian craton (assuming that the north Australian and west Australian cratons had amalgamated at that time; see discussion in Wingate & Evans 2003) suggests a likely age of ∼1.6 Ga for the HP1 direction.

Our ChRM2 pole does not resemble the regional 'pervasive ∼1.7 Ga overprint' direction, but lies close to the HP1 pole of Li *et al.* (2000), in the vicinity of the ∼1.5–1.6 Ga segment of the APWP of Wingate & Evans (2003). The confidence limits for our ChRM2 palaeopole do not intersect the APWP of Wingate & Evans (2003). However, taking into consideration that the APWP for this time period is based on a small data set and, thus, is of low precision, a ∼1.5 Ga age for the remanence cannot be excluded.

An alternative age range for the ChRM2 remanence is suggested by its general similarity with middle to late Palaeozoic directions. The strict comparison, however, is hampered by the contentious nature of the Australian APWP for this time interval (see discussions in Schmidt *et al.* 1990; Klootwijk 2009). Different approaches to interpretation of palaeomagnetic data, particularly concerning whether

Table 3. Palaeomagnetic poles reported from iron ore deposits of the Hamersley province.

Locality		*N*	Plat	Plong	d*p*	d*m*	Reference
Mount Tom Price	(TP'94)	19	−37.4	220.3	5.7	11.3	Schmidt & Clark (1994)
Mount Tom Price	(TP'68)	28	−22.0	237.0	12.0	12.0	Porath & Chamalaun (1968)
Paraburdoo	(PBD)	15	−36.4	209.9	4.7	8.8	Schmidt & Clark (1994)
Mount Newman	(MN'68)	20	−17.0	246.0	9.5	9.5	Porath & Chamalaun (1968)
Hamersley province overprint	(HP1)	17	−33.9	70.7	8.4	8.4	Li *et al.* (2000)
Hamersley province overprint	(HP2)	38	−35.3	211.9	3.0	3.0	Li *et al.* (2000)
Pilbara Print Stone	ChRM1	27	−82.2	126.7	3.0	4.5	This study
Pilbara Print Stone	ChRM2	16	−48.6	88.0	4.8	5.5	This study

Notes: N is the number of samples; Plat, palaeopole latitude (in °); Plong, palaeopole longitude (in °); d*p* and d*m* are semi-axes of the 95 per cent cone of confidence about the mean (in °). Instead of defining palaeopole confidence limits in k and A_{95} (assuming a Fisherian virtual geomagnetic pole distribution), we, for consistency, follow the convention of the referenced publications by using d*p* and d*m* (assuming a Fisher (1953) distribution of palaeomagnetic directions).

reported directions are recognized as primary magnetizations or as overprints, have led to two widely different APWP options for Australia; a clockwise path (Li *et al.* 1990; Schmidt *et al.* 1990), which is usually referred to as the SLP-type (Schmidt-Li-Powell) path following the terminology of Klootwijk (2009), and an alternative counter-clockwise KG path of Klootwijk & Giddings (1988).

Our ChRM2 pole lies in the vicinity of the Late Carboniferous segment in both paths; the best fit is achieved at ∼323 Ma in the SLP-type APWP (Fig. 10c), and at ∼310 Ma in the KG APWP (Fig. 10d). Secondary magnetizations of middle Carboniferous age, which are temporally associated with the polyphase ∼450–300 Ma intraplate Alice Springs orogeny, are common in Australia (e.g. Schmidt *et al.* 1987; Klootwijk 2010). Several pulses of Mississippi Valley-type mineralization in Western Australia, all temporally coinciding with the waning stages of the Alice Springs orogeny (Tompkins *et al.* 1997), point to vast hydrothermal fluid flow through the crust at that time (e.g. Leach *et al.* 2001). The Newsprint pigment of the PPS that carries the ChRM2 remanence may have precipitated during one such hydrothermal pulse.

To summarize, comparison with existing APWP options for Australia allows two possible time intervals for acquisition of the ChRM2 direction; Mesoproterozoic (∼1.5 Ga) and Late Carboniferous (∼325–310 Ma). Considering the 2.5 Ga depositional age of the McRae Shale that provides matrix for the pigment, a known history of iron-rich fluid transport in the region, and uncertainties in the Australian APWP, we are unable to provide a conclusive preference for either alternative.

6.2 Pigment characteristics

The difference in pigment distribution in the Newsprint and uniform types in the PPS samples points to different interactions between matrix rocks and iron-bearing fluids (e.g. Jamtveit & Hammer 2012). Locally, concentric and parallel stripes with gentle curvature of the Newsprint type (Fig. 1b) are reminiscent of Liesegang banding (Liesegang 1896). Although formation of this type of pattern is not completely understood (e.g. Krug *et al.* 1996), it has been suggested that iron oxide precipitation relates to oxygen diffusion into regions in which iron was dissolved in pore waters (e.g. McBride 2003; Barge *et al.* 2011). On the other hand, the hieroglyphic pattern with angular corners, such as the picture resembling the Chinese character Tao, a 'path', in the left-hand side of Fig. 1(c), as well as deposition of pigment along the bedding surfaces (Figs 1b and c), suggests that pigment distribution was controlled by solute transport pathways, such as through a system of fractures or a porosity network. In a confined environment of a sedimentary bed, such fluid transport pathways can be generated and maintained when chemical reactions result in a reduction of matrix volume, or, alternatively, by fracturing associated with increased matrix volume (e.g. Eichhubl 2004; Jamtveit & Hammer 2012).

The contrasting modes of pigment distribution suggest that sedimentary pores and capillaries, which were largely closed at the time of Newsprint deposition became open to iron-bearing fluids at the time of uniform pigment formation. This, in turn, suggests differences in hydrostatic pressure (burial depth) and/or fluid chemistry, and, by extension, a large time difference between pigment precipitation episodes. While the large overlap in coercivities and unblocking temperatures between the Newsprint and uniform pigments (Fig. 7b) hampers use of magnetic parameters for identifying the dominant pigment type in a particular specimen, the association of distinct palaeomagnetic directions with the PPS pigment types is helpful. Both the ChRM1 and ChRM2 groups include antipodal directions that are indicative of prolonged, spanning at least one geomagnetic polarity transition, growth of pigment grains. The statistically significant difference between the mean ChRM1 and ChRM2 directions (i.e. their confidence limits do not overlap) is consistent with pigment growth (remanence acquisition) at different times. No 'intermediate' ChRM directions are observed, although some changes in vector end-point trajectories in the lower (300–550 °C) unblocking temperature range (e.g. Fig. 2) may represent such composite directions.

The PDF-like directions carried by goethite suggest that goethite precipitation was a recent phenomenon, likely related to surface weathering/oxidation. Recording of a reversed polarity direction by fine haematite grains (a low coercivity component removed by AF demagnetization, Fig. 3) is inconsistent with the low coercivity remanence being a viscous remanent magnetization that would be expected to record a PDF direction; more likely, it represents a chemical remanence acquired during a reversed polarity geomagnetic interval. Lack of PDF directions recorded by fine-grained haematite (e.g. Fig. 3) indicates that haematite growth was either suppressed or was much slower than goethite growth under present environmental conditions.

Whether the older ChRM2 remanence is preserved in a particular specimen seems to depend on colour density (concentration) of the uniform 'background' pigment. Colour and blocking temperature depend on haematite grain volume (e.g. Cornell & Schwertmann 2003), therefore, such a correlation points to protracted pigment formation for the uniform pigment. Grains that nucleated early and continued to grow would have reached volumes and concentrations comparable with those of the Newsprint pigment (with high

unblocking temperatures). Grains that nucleated later (or whose growth was aborted by reduced iron supply due, for example, to diversion of fluid flow), would have grown to smaller volumes with lower maximum unblocking temperatures, and thus would not be able to completely overprint the earlier ChRM2. In contrast to the strict association between remanence direction and pigment type in the PPS samples, multistage pigment growth produced composite magnetization directions in the TOM specimens. The linear composite components are likely due to nearly identical unblocking temperature spectra (grain size distributions) of haematite grains that grew during the respective normal and reverse polarity episodes.

6.3 Palaeomagnetic implications of haematite pigmentation

In the uniform pigment, several features, including large variations in the content of goethite and the finest-grained haematite (that is responsive to AF demagnetization, Fig. 3), different ChRM directions for specimens from the same PPS hand-samples (Table 1), and the large angular separation between composite ChRM directions for the TOM collection, collectively highlight large-scale short-range (cm-scale) variability in pigment precipitation patterns. Such variability implies a strong local control on pigment formation. By extension, our findings suggest that diagenetic precipitation of haematite pigment, which is evident, for example, in the red colour of rocks, might not necessarily result in complete remagnetization of sedimentary sequences. It is likely that some pockets within sedimentary formations will be less affected by pigment formation and might preserve an earlier palaeomagnetic signal. Preservation of the distinctive Newsprint remanence associated with an early fluid migration episode in some samples in our collection, or the observation of Liu *et al.* (2011) that ∼7 per cent of their studied Lower Triassic red beds preserved a primary ChRM while the rest carried a secondary magnetization residing in haematite pigment, suggest that local persistence of a primary palaeomagnetic signal in red bed sequences could be more common than is often thought to be the case.

However, it can be difficult to confirm whether haematite remanences are primary. Positive reversal tests for both types of Print Stone pigment highlight the ambiguity of the reversal test in haematite-bearing rocks (e.g. Derder *et al.* 2001; Henry *et al.* 2004). Care should, therefore, be taken when interpreting dual polarity magnetizations residing in haematite as an indication of primary remanence.

7 CONCLUSIONS

Our study of different haematite pigment types found in the ∼2.5 Ga McRae Shales, Hamersley Basin, Western Australia, suggests that precipitation of pigment temporally coincided with known episodes of regional fluid migration. Two distinct populations of remanence directions, each consisting of antipodal groups, can be correlated to pigment type within the studied PPS sample collection. The ChRM1 remanence carried by the uniform pigment can be dated to ∼15–25 Ma by comparison with the Australian APWP. For the ChRM2 remanence that resides in the Newsprint pigment, two age options are permissible; a Mesoproterozoic (∼1.5 Ga) or middle Carboniferous (∼320–310 Ma) pigmentation. In the TOM samples, the ChRM directions appear to follow great circle trends that converge on a direction close to the ChRM2 direction of the PPS sample collection.

There are bulk rock magnetic differences between the Newsprint and uniform pigment types, such as higher M_r/M_s, B_c and B_{cr} values in the Newsprint pigment. Also, goethite is present in the uniform pigment, but not in the Newsprint pigment. A wide overlap in coercivity spectra between the pigment types restricts use of rock magnetic parameters for unambiguous discrimination between the types. Nevertheless, the recorded palaeomagnetic directions enable clear discrimination between pigment types.

In the studied sedimentary rocks, uniformly coloured pigment has highly variable (on a centimetre scale) goethite content and haematite grain size, and, thus, remanence carrying capacity. Such short-range large-scale variability implies a strong local control on pigment formation, which raises the possibility that an early (primary) remanent magnetization may survive in local pockets within sedimentary red bed formations.

ACKNOWLEDGEMENTS

We sincerely thank Barry Kayes, Director of Aradon Pty Ltd, Perth, for permission to sample the Print Stone, the Geological Survey of Western Australia and the geological team of the Tom Price Mine for logistical and moral support during field work, Xiang Zhao for translation of Chinese characters, and Bernard Henry and the journal Editor Andrew Biggin for constructive review comments.

REFERENCES

Anbar, A.D., Duan, Y., Lyons, T.W., Arnold, G.L., Kendall, B., Creaser, R.A. & Buick, R., 2007. A whiff of oxygen before the great oxidation event?, *Science,* **317,** 1903–1906.

Anderson, K.L., Lackie, M.A., Clark, D.A. & Schmidt, P.W., 2004. Return to Black Mountain: palaeomagnetic reassessment of the Chatsworth and Ninmaroo formations, western Queensland, Australia, *Geophys. J. Int.,* **157,** 87–104.

Barge, L.M., Hammond, D.E., Chan, M.A., Potter, S., Petruska, J. & Nealson, K.H., 2011. Precipitation patterns formed by self-organizing processes in porous media, *Geofluids,* **11,** 124–133.

Carter-Stiglitz, B., Banerjee, S.K., Gourlan, A. & Oches, E., 2006. A multiproxy study of Argentina loess: marine oxygen isotope stage 4 and 5 environmental record from pedogenic haematite, *Palaeogeogr. Palaeoclimatol. Palaeoecol.,* **239,** 45–62.

Chadima, M. & Hrouda, F., 2006. Remasoft 3.0 a user-friendly paleomagnetic data browser and analyser, *Travaux Géophys.,* **27,** 20–21.

Cornell, R.M. & Schwertmann, U., 2003. *The Iron Oxides: Structure, Properties, Reactions, Occurrences and Uses,* Wiley-VCH.

Dang, M.Z., Rancourt, D.G., Dutrizac, J.E., Lamarche, G. & Provencher, R., 1998. Interplay of surface conditions, particle size, stoichiometry, cell parameters, and magnetism in synthetic haematite-like materials, *Hyperfine Interact.,* **117,** 271–319.

Danišík, M., Evans, N.J., Ramanaidou, E.R., McDonald, B.J., Mayers, C. & McInnes, B.I., 2013. (U-Th)/He chronology of the Robe River channel iron deposits, Hamersley Province, Western Australia, *Chem. Geol.,* **354,** 150–162.

Dekkers, M.J., 1989. Magnetic properties of natural goethite—I. Grain-size dependence of some low-and high-field related rock magnetic parameters measured at room temperature, *Geophys. J. Int.,* **97,** 323–340.

Derder, M.E.M., Henry, B., Merabet, N., Bayou, B. & Amenna, M., 2001. Paleomagnetism of the Liassic member of the Zarzaïtine Formation (stable Saharan craton, Illizi basin, Algeria), *Annal. Geofis.,* **44,** 994–1010.

Dunlop, D.J. & Özdemir, Ö., 1997. *Rock Magnetism: Fundamentals and Frontiers,* Cambridge Univ. Press.

Eichhubl, P., 2004. Growth of ductile opening-mode fractures in geomaterials, *Geol. Soc. Lond. Spec. Publ.,* **231,** 11–24.

Fisher, R.A., 1953. Dispersion on a sphere, *Proc. R. Soc. Lond. A,* **217,** 295–305.

Harmsworth, R.A., Kneeshaw, M., Morris, R.C., Robinson, C.J. & Shrivastava, P.K., 1990. BIF derived iron ores of the Hamersley Province, in *Geology of the Mineral Deposits of Australia and Papua New Guinea,* pp. 617–642, ed. Hughes, F.E., The Australian Institute of Mining and Metallurgy.

Henry, B., Merabet, N., Derder, M.E.M. & Bayou, B., 2004. Chemical remagnetizations in the Illizi basin (Saharan craton, Algeria) and their acquisition process, *Geophys. J. Int.,* **156,** 200–212.

Heslop, D. & Roberts, A.P., 2012. Estimation of significance levels and confidence intervals for first-order reversal curve distributions, *Geochem. Geophys. Geosyst.,* **13,** Q12Z40, doi:10.1029/2012GC004115.

Jamtveit, B. & Hammer, Ø., 2012. Sculpting of rocks by reactive fluids, *Geochem. Perspect.,* **1,** 341–481.

Kirschvink, J.L., 1980. The least-squares line and plane and the analysis of palaeomagnetic data. *Geophys. J. R. astr. Soc.,* **62,** 699–718.

Klootwijk, C., 2009. Sedimentary basins of eastern Australia: paleomagnetic constraints on geodynamic evolution in a global context, *Aust. J. Earth Sci.,* **56,** 273–308.

Klootwijk, C., 2010. Australia's controversial Middle-Late Palaeozoic pole path and Gondwana–Laurasia interaction, *Palaeoworld,* **19,** 174–185.

Klootwijk, C.T. & Giddings, J.W., 1988. An alternative APWP for the Middle to Late Palaeozoic of Australia—implications for terrane movements in the Tasman Fold Belt, *Geol. Soc. Aust. Abstr.,* **21,** 219–220.

Kobayashi, K., 1962. Magnetization-blocking process by volume development of ferromagnetic fine particles, *J. Phys. Soc. Jpn,* **17,** 695–698.

Krug, H.-J., Brandtstadter, H. & Jacob, K.H., 1996. Morphological instabilities in pattern formation by precipitation and crystallization processes, *Geol. Rundsch.,* **8,** 19–28.

Kruiver, P.P., Dekkers, M.J. & Heslop, D., 2001. Quantification of magnetic coercivity components by the analysis of acquisition curves of isothermal remanent magnetisation. *Earth planet. Sci. Lett.,* **189,** 269–276.

Leach, D.L., Bradley, D., Lewchuk, M.T., Symons, D.T., de Marsily, G. & Brannon, J., 2001. Mississippi Valley-type lead–zinc deposits through geological time: implications from recent age-dating research, *Mineral. Deposita,* **36,** 711–740.

Li, Z.X., Guo, W. & Powell, C.M., 2000. Timing and genesis of Hamersley BIF-hosted iron deposits: a new palaeomagnetic interpretation, in *MERIWA Project M242 Final Report,* Tectonics Special Research Centre, UWA, Nedlands, Western Australia, pp. 1–283.

Li, Z.X., Powell, C.M., Thrupp, G.A. & Schmidt, P.W., 1990. Australian Palaeozoic palaeomagnetism and tectonics—II. A revised apparent polar wander path and palaeogeography, *J. Struct. Geol.,* **12,** 567–575.

Li, Z.X., Powell, C.M. & Bowman, R., 1994. Timing and genesis of Hamersley iron-ore deposits, *Explor. Geophys.,* **24,** 631–636.

Liesegang, R., 1896. Ueber einige eigenschaften von gallerten, *Naturwiss. Wochenschr.,* **10,** 353–362.

Liu, C., Ge, K., Zhang, C., Liu, Q., Deng, C. & Zhu, R., 2011. Nature of remagnetization of Lower Triassic red beds in southwestern China, *Geophys. J. Int.,* **187,** 1237–1249.

Liu, Q., Yu, Y., Torrent, J., Roberts, A.P., Pan, Y. & Zhu, R., 2006. Characteristic low-temperature magnetic properties of aluminous goethite [α-(Fe, Al) OOH] explained, *J. geophys. Res.,* **111,** B12S34, doi: 10.1029/2006JB004560.

Macphail, M.K. & Stone, M.S., 2004. Age and palaeoenvironmental constraints on the genesis of the Yandi channel iron deposits, Marillana Formation, Pilbara, northwestern Australia, *Aust. J. Earth Sci.,* **51,** 497–520.

McBride, E.F., 2003. Pseudofaults resulting from compartmentalized Liesegang bands: update, *Sedimentology,* **50,** 725–730.

McFadden, P.L. & McElhinny, M.W., 1990. Classification of the reversal test in palaeomagnetism. *Geophys. J. Int.,* **103,** 725–729.

Morin, F.J., 1950. Magnetic susceptibility of alpha-Fe_2O_3 and alpha-Fe_2O_3 with added titanium, *Phys. Rev.,* **78,** 819–820.

Özdemir, Ö. & Dunlop, D.J., 1996. Thermoremanence and Néel temperature of goethite, *Geophys. Res. Lett.,* **23,** 921–924.

Özdemir, Ö., Dunlop, D.J. & Berquó, T.S., 2008. Morin transition in hematite: size dependence and thermal hysteresis, *Geochem. Geophys. Geosyst.,* **9,** Q10Z01, doi:10.1029/2008GC002110.

Park, J.K., 1997. Paleomagnetic evidence for low-latitude glaciation during deposition of the Neoproterozoic Rapitan Group, Mackenzie Mountains, NWT, Canada, *Can. J. Earth Sci.,* **34,** 34–49.

Pickard, A.L., Barley, M.E. & Krapež, B., 2004. Deep-marine depositional setting of banded iron formation: sedimentological evidence from interbedded clastic sedimentary rocks in the early Palaeoproterozoic Dales Gorge Member of Western Australia, *Sediment. Geol.,* **170,** 37–62.

Pike, C.R., Roberts, A.P. & Verosub, K.L., 1999. Characterizing interactions in fine magnetic particle systems using first order reversal curves, *J. appl. Phys.,* **85,** 6660–6667.

Porath, H. & Chamalaun, F.H., 1968. Palaeomagnetism of Australian haematite orebodies. II. Western Australia, *Geophys. J. R. astr. Soc.,* **15,** 253–264.

Raiswell, R., Reinhard, C.T., Derkowski, A., Owens, J., Bottrell, S.H., Anbar, A.D. & Lyons, T.W., 2011. Formation of syngenetic and early diagenetic iron minerals in the late Archean Mt. McRae Shale, Hamersley Basin, Australia: new insights on the patterns, controls and paleoenvironmental implications of authigenic mineral formation, *Geochim. Cosmochim. Acta,* **75,** 1072–1087.

Rasmussen, B., Fletcher, I.R. & Sheppard, S., 2005. Isotopic dating of the migration of a low-grade metamorphic front during orogenesis, *Geology,* **33,** 773–776.

Rasmussen, B., Fletcher, I.R., Muhling, J.R., Thorne, W.S. & Broadbent, G.C., 2007. Prolonged history of episodic fluid flow in giant haematite ore bodies: evidence from in situ U–Pb geochronology of hydrothermal xenotime, *Earth planet. Sci. Lett.,* **258,** 249–259.

Rath, C., Sahu, K.K., Kulkarni, S.D., Anand, S., Das, R.P. & Mishra, N.C., 1999. Microstructure-dependent coercivity in monodispersed haematite particles, *Appl. Phys. Lett.,* **75,** 4171–4173.

Ricordel, C., Parcerisa, D., Thiry, M., Moreau, M.G. & Gómez-Gras, D., 2007. Triassic magnetic overprints related to albitization in granites from the Morvan massif (France), *Palaeogeogr. Palaeoclimatol. Palaeoecol.,* **251,** 268–282.

Roberts, A.P., Cui, Y. & Verosub, K.L., 1995. Wasp-waisted hysteresis loops: mineral magnetic characteristics and discrimination of components in mixed magnetic systems, *J. geophys. Res.,* **100,** 17 909–17 917.

Roberts, A.P., Pike, C.R. & Verosub, K.L., 2000. First-order reversal curve diagrams: a new tool for characterizing the magnetic properties of natural samples, *J. geophys. Res.,* **105,** 28 461–28 475.

Roberts, A.P., Liu, Q., Rowan, C.J., Chang, L., Carvallo, C., Torrent, J. & Horng, C.S., 2006. Characterization of hematite (α-Fe_2O_3), goethite (α-FeOOH), greigite (Fe_3S_4), and pyrrhotite (Fe_7S_8) using first-order reversal curve diagrams, *J. geophys. Res.,* **111,** B12S35, doi:10.1029/2006JB004715.

Robertson, D.J. & France, D.E., 1994. Discrimination of remanence-carrying minerals in mixtures, using isothermal remanent magnetisation acquisition curves, *Phys. Earth planet. Inter.,* **82,** 223–234.

Schmidt, P.W. & Clark, D.A., 1994. Palaeomagnetism and magnetic anisotropy of Proterozoic banded-iron formations and iron ores of the Hamersley basin, Western Australia, *Precambrian Res.,* **69,** 133–155.

Schmidt, P.W., Embleton, B.J.J. & Palmer, H.C., 1987. Pre-and post-folding magnetizations from the early Devonian Snowy River Volcanics and Buchan Caves Limestone, Victoria, *Geophys. J. R. astr. Soc.,* **91,** 155–170.

Schmidt, P.W., Powell, C.M., Li, Z.X. & Thrupp, G.A., 1990. Reliability of Palaeozoic palaeomagnetic poles and APWP of Gondwanaland, *Tectonophysics,* **184,** 87–100.

Stoner, E.C. & Wohlfarth, E.P., 1947. Interpretation of high coercivity in ferromagnetic materials, *Nature,* **160,** 650–651.

Tauxe, L., Mullender, T.A.T. & Pick, T., 1996. Potbellies, wasp-waists, and superparamagnetism in magnetic hysteresis, *J. geophys. Res.,* **101,** 571–583.

Taylor, D., Dalstra, H.J., Harding, A.E., Broadbent, G.C. & Barley, M.E., 2001. Genesis of high-grade haematite orebodies of the Hamersley Province, Western Australia, *Econ. Geol.,* **96,** 837–873.

Tompkins, L.A., Eisenlohr, B., Groves, D.I. & Raetz, M., 1997. Temporal changes in mineralization style at the Cadjebut Mississippi valley-type deposit, Lennard Shelf, WA, *Econ. Geol.,* **92,** 843–862.

Torsvik, T.H., Müller, R.D., Van Der Voo, R., Steinberger, B. & Gaina, C., 2008. Global plate motion frames: toward a unified model, *Rev. Geophys.,* **46,** 1–44.

Trendall, A.F. & Blockley, J.G., 1970. The iron formations of the Precambrian Hamersley Group, Western Australia: with special reference to the associated crocidolite, *West. Aust. Geol. Surv. Bull.,* **119,** 336.

Van Der Voo, R. & Torsvik, T.H., 2012. The history of remagnetization of sedimentary rocks: deceptions, developments and discoveries, *Geol. Soc. Lond. Spec. Publ.,* **371,** 23–53.

Wagner, C., Orberger, B., Tudryn, A. & Wirth, R., 2013. Fluid-induced martitization of magnetite in BIFs from the Dharwar Craton, India, *European Geosciences Union General Assembly,* Vienna, Austria, Geophys. Res. Abst., EGU2013-7973-2.

Wingate, M.T. & Evans, D.A., 2003. Palaeomagnetic constraints on the Proterozoic tectonic evolution of Australia. *Geol. Soc. Lond. Spec. Publ.,* **206,** 77–91.

Zijderveld, J.D.A., 1967. A.C. demagnetization of rocks, in *Methods in Palaeomagnetism,* pp. 256–286, eds Collinson, D.W., Creer, K.M. & Runcorn, S.K., Elsevier.